Image Splicing Forgery Detection Model Using Hybrid Boosting Machine

Meena Ugale, J. Midhunchakkaravarthy

***Abstract*—The rapid evolution of technology has raised questions about the authenticity of digital images due to easy access to software for image manipulation. This challenges the reliability of cybernetic images, making it difficult for analysts to verify their authenticity. Therefore, there is a need to improve image forgery detection techniques. Many existing systems rely on standard pooling and a single approach, limiting the comprehensiveness and demonstration of features acquired. In response, this research introduces a Pixel-Based Optimized Deep Convolutional Neural Network (PBO-DCNN) classification and a Hybrid Boosting Machine method for detecting image fabrications. The technique employs block-wise feature extraction in a block-by-block manner and a Hybrid Boosting Machine segmentation approach to enhance detection. Performance analysis shows that the Hybrid Boosting Machine approach attained an accuracy of 94.74%, a sensitivity of 95.00%, and a specificity of 95.27% on the DSO-1 dataset. Further, the Hybrid Boosting Machine model attained the accuracy, sensitivity, and specificity values of 94.86%, 94.97%, and 93.38% on the DSI-1 dataset concerning the training percentage (TP). Comparative analysis against traditional techniques such as Linear Regression (LR), Deep CNN, SVM, Decision Tree (DT), and Naïve Bayes (NB) classifiers demonstrates the superior performance of the Hybrid Boosting Machine approach.**

***Index Terms*—Deep CNN, Forgery detection, Feature extraction, Hybrid Boosting Machine, Segmentation.**

I. INTRODUCTION

The human brain possesses a remarkable ability to process and understand visual details, which finds applications in diverse domains such as education, the internet, healthcare, law, entertainment, and more. With the proliferation of image editing tools on portable devices like smartphones and laptops, there is a growing potential for image manipulation for various purposes, which can significantly impact public perception [1]. Consequently, it becomes essential to establish techniques for detecting image tampering and falsification. Typically, image falsification is divided into three categories: imitation [9], integration [10], and deletion [11].

Imitation involves copying elements from one image and pasting them into another, while integration separates and combines image elements from different sources. Deletion, on the other hand, entails removing a portion of an image and replacing it with a pixel pattern [2].

The advent of user-friendly image editing applications has made it easier to alter image content, and image falsification can occur virtually anywhere.

This rise in image manipulation coincides with the increasing prevalence and sophistication of manipulated images, making it a significant concern. Detecting and determining image falsification is a global problem, as it involves distinguishing characteristics among various regions of images to identify tampered sections [6]. Automated image falsification can be broadly categorized into two types: imitation and interlace falsification. In imitation falsification, portions of image elements are transposed into similar images, whereas interlace falsification involves borrowing elements from other images to create the manipulated image [3]. Depending on the alteration of the visual components of an image, falsification can be broadly categorized into global falsification [12][13] and local falsification.

In global falsification, imitation, and deletion falsification impact a single source image, while interlace falsification combines parts from one or multiple source images into the target image [4]. These manipulations can often be achieved without leaving clear evidence and can be challenging for the human eye to detect. These manipulations can be executed using various techniques, including imitation, interlacing, and modification. These methods involve integrating various portions of one or more images to produce a new image [5]. Recently, images with proximity and easily understandable visual elements have become a primary source of news dissemination and are used as evidence in legal proceedings, investigative work, public forums, and real-time events. For interlace falsification, regions are typically distorted, rearranged, and obscured to create a manipulated image, making it difficult for the human eye to detect these falsifications [8]. Support vector data description is utilized by Ayoub Mniai and Khalid Jebari [20] for credit card fraud detection. Hirofumi Miyajima [21] et al., used the ML algorithm along with the PSO to secure the data in the cloud and edge systems.

As for the models based on CNN, various techniques [6] majorly study the variations among the image patch to decide if an image patch is influenced or not. For example, the research [6] developed a two-phase identification system, which digests the variations of the image elements identification system based on CNN, the researchers normally utilize usual pooling performance such as max-pooling and mean-pooling to condense the features, but these functions will lead to the loss of information, which is irrevocable. As the details of the educated attributes are misplaced, it will be a severe challenge for the systems to identify the trespassed areas by differentiating the attribute variations of every pictorial area. Furthermore, they only concentrate on a particular undertaking, like creating the identified trespassed areas, which assembles the attributes

Manuscript received August 31, 2023; revised April 27, 2024.

Meena Ugale is a PhD Student at Department of Computer Science and Multimedia, Lincoln University College, Kuala Lumpur 47301, Malaysia (email: meena.u@xavier.ac.in)

J. Midhunchakkaravarthy is Associate Professor, Faculty of Computer Science and Multimedia, Lincoln University College, Kuala Lumpur 47301, Malaysia (email: midhun@lincoln.edu.my)

studied by the network system into more provisional as well as fewer representative [6], and it has been discovered that the search field didn't pass its developing phase yet and emerged as a theme of curiosity for various types of research, in which the traditional techniques [8] were utilized. The image interlacing fabrication is identified either by the combination of DWT and LBP [8] or Markov and DWT fusion [8], however, as per the author's better intelligence, the fusion of DWT, Markov, and LBP were yet to be utilized in the applications [8].

The key intention of the research is image forgery detection, in which the data needed for the identification of forgery is collected from the dataset [14], and then the preprocessing is employed to make the input image useful for the forgery identification. A Hybrid Boosting Machine as well as a Pixel-based optimized deep CNN is developed to identify the input image as normal or forged.

- ***Hybrid Boosting Machine:*** The Hybrid Boosting Machine is established based on the conventional hybridization of the light Gradient Boosting Machine (light GBM) technique and the Decision Tree (DT), which will detect whether the inserted image is normal or forged.
- ***Pixel-Based Optimized Deep Convolutional Neural Network (PBO-DCNN):*** The pixel-based optimized deep CNN classification algorithm identifies the information of the picture elements of the forged imagery and presents the segmented picture element to the classification process. The further process will be in between the real image in the increased test blocks and the fabricated picture elements given by the pixel-based deep CNN algorithm and the forged image will be sectioned.

The image forgery detection method presented in the previous papers with its pros and cons are explained in section II, and the proposed Pixel-based optimized deep CNN and Hybrid Boosting Machine are enumerated in section III. The output achieved is projected in section IV and the conclusion is depicted in section VIII.

II. Literature Review

Several previous research based on the detection of image forgery were reviewed and described in this section with their benefits as well as drawbacks.

Kalyani Kadam *et al.* in [1] developed a multi-image interlacing identification by utilizing the Mask Refined-CNN (RCNN), along with the MobileNet V1 as a vertebra to detect and label a numerous image interlacing falsification with the increased rate of identification and reduced size of the technique as well as complexity, and estimates the probability of an artificial area of multi-interlace pictures. However, the established model takes an extended period for the process. Hongwei Ding *et al.* in [2] established the advanced image interfere location technique based on double-channel U-Net (DCU-Net), in which the identification structure based on the technique is primarily separated into three sections such as encipher, feature connection, as well as decipher, where the method input is the real trespassed picture as well as the tampered remaining image, and the fusion of the feature for identifying the image interlacing fabrication, where the experimental analysis states that the method reduces the information loss as well as memory consumption. However, the mathematical complexity of the technique is huge. Moreover, in [3] Bin Xiao *et al.* suggested an identification technique for interlacing fabrication with two sections such as a coarse-to-RCNN (C2RNet) as well as dilute adaptive clustering, which issues a coarse-CNN as RCNN, and removes the variations present in the image elements among the interfered and un-interfered areas from the image patch with various lengths. However, the concentration of the machine sound is feeble and the identification method might happen to be void. In [4] Bo Liu*et et al.* developed the D-Unet model for image interlace identification, which uses a detached and stable encipher, which is succeeded by a spatial feature extraction technique, which lengthens the universal perception of D-Unetto and categorize the interfered and un-interfered areas. It decreases the failure identification range, high precision, F-measure, and high recall range. However, the technique improves the complexity of identification as the changing function regularly misses some images. Sahani Pooja Jaiprakash *et al.* [5] developed a low-dimensional feature-based technique to substantiate the images and to access the areas diagnosis by utilizing the novel key-point-based technique; its experimental outcome shows that the approach decreased the time of detection and detected the dual kind of non-resistance at the similar period. This method is not suitable for compositing functions. Xiuli Bi *et al.* in [6] developed a multiple-task wavelet corrected network (MWC-Net) that could learn many extensive and indicative attributes for the identification of image interlacing and locating, in which the method makes use of wavelet-pooling and un-pooling to reduce and renovate the attributes of fabricated images, which decreases the loss of information. However, the technique will not be utilized in the alternative functions of pooling. In [7] Avinash Kumar *et al.* implemented an improved Markov technique in the Block Discrete Cosine Transform (BDCT) field and the Discrete Meyer Wavelet Transform (DMWT) field to categorize the forged image from a real image; the cross-field attributes stimulate the last critical attributes for Support Vector Machine (SVM) algorithm which reduces the size of the feature vector length at a less computational price. However, a large number of attributes create over-fitting issues. In [8] Navneet Kaur *et al.* extracted and merged both the DWT and the LBP fields for the identification of image forging, in which the three-stage DWT is implied to the original image with separate Haar wavelet, which achieved additional information and a little amount of noise, with reduced computational complexity. However, the method contains high computation expenses. In [22] Kang Tan *et al.* introduced an image manipulation method utilizing a two-stream Faster R-CNN architecture with a constrained convolution layer in the preprocessing stage by incorporating the Convolutional Block Attention Module (CBAM) into the model to improve the attention towards tampered regions, allowing the model to focus on a larger manipulation area within the image.

Challenges

a. The MobileNet V1 technique is required to be evaluated with different attacks and will differentiate the estimated outcomes either in the presence or absence of the ambush [1].
b. The DCU-Net technique is required to be integrated with object detection techniques such as RCNN and YOLO

methods to resolve the issue regarding the functioning imagery by analyzing the possible varying attributes among the interfering or non-interfering region and a broader identification method will also be generated [2].

c. The C2RNet model is to be focussed only on an individual interfered area in imagery due to the limitation of the post-processing technique, and the problem will be evaluated and eliminated in the upcoming research.

d. The passive approach is to be further implied to the medicinal imagery that makes it useful for the local civilization as well as the research group of people [8].

III. Methodology

The major purpose of this paper is to recognize the image splicing as well as to section the fabricated imagery by utilizing the Hybrid Boosting Machine and Pixel-Based Optimized Deep CNN classifier.

At first, the input image will be composed of the image forgery detection dataset (DTS) known as DSO-1 and DSI-1[14] which will be further passed to pre-processing to decrease the noise and data irregularity. The block-wise feature extraction and the ResNet 101 feature extraction will be conducted simultaneously. The real imagery is altered to YCbCr to utilize the lesser declaration potential of the human vision network for color proportional to the luminosity, and then after the alteration and extraction of the ResNet 101 feature map, the attributes will be integrated and passed to the pixel-based optimized deep CNN classifier, in which the feature extraction is functioned by the feature progression like the Haralick feature, Local ternary pattern, SIFT, and light coefficient features.

Haralick feature is the process of the standard Grey Level Co-occurrence Matrix (GLCM), whereas the local ternary pattern utilizes threshold stability to threshold components into three integrities, and the SIFT feature is utilized to identify and explain the general image attributes. The light coefficient attributes estimate the effectiveness, and then the features are sequenced. Simultaneously, the block-wise feature extracted will be further passed to the novel Hybrid Boosting Machine established by the conventional hybridization of the light GBM and Decision Tree (DT).

Moreover, the Hybrid Boosting Machine will identify the input image as normal or forged, and if the detected imagery is evaluated to be forged, it will be passed to the PBO-DCNN classifier.

The normal data will be passed to the enlarged blocks, in which the PBO-DCNN classifier detects the pixel details of the fabricated imagery and offers the sectioned pixel to the Hybrid Boosting Machine. The differentiation will function among the real image in the increased test blocks and the fabricated pixels provided by the PBO-DCNN classifier and the fabricated image will be sectioned.

The research will be carried out by utilizing PYTHON and effectiveness will be evaluated concerning the performance metrics which include accuracy, sensitivity, specificity, and segmentation accuracy. The diagrammatic demonstration of the Hybrid Boosting Machine methodology is shown in Fig.1.

A. Data Collection

The input image employed in this paper is collected from the DTS DSO-1 and DSI-1 [14] which include 200 inside as well as exterior images along with an image assertion of 2,048 x 1,536 picture elements, which is expressed arithmetically as,

$$D_t = IM_{fd} \tag{1}$$

where, D_t is referred to as a dataset and IM_{fd} is specified as image forgery.

B. Image Preprocessing

The data preprocessing is functioned for reducing the unnecessary noise present in the data collected from the database [14], thus, the attributes might be efficiently extracted for the recognition of the forged image, in which the pre-processed image is articulated by,

$$D_t^* = IM_{fd}^* \tag{2}$$

where, D_t is referred to as a dataset and IM_{fd} is specified as image forgery.

C. Block-wise Feature Extraction

The computer radiography (CR) based categorization system normally utilizes original image elements which are vectorized as an attribute vector. Nevertheless, these techniques essentially need the test image and the training image to be associated well, in which, if the test imagery contains a smaller number of listing issues adjacent to the training imagery, the demonstration factors will be no longer instructive. Therefore, to handle this issue, various research was performed in recent times. The block-wise statistics which involves Haralick features, LTP, scale-invariant feature transform (SIFT), and light coefficient features is developed.

D. Haralick features

The Haralick features (HF) are used as general surface signifiers in the image analysis. To calculate these features, the image's gray levels are reduced through a process known as quantization. Since the subsequent features heavily depend on the quantization processes, the HFs are irreproducible if a similar quantization fails. These features are counted using the GLCM, which signalizes the surface by refactoring the frequent occurrence of the sets of adjacent picture elements with specific rates. Additionally, the GLCM is regulated by the number of gray levels present in the quantized imagery and affects the rates of the surface attributes. With increasing number of gray levels, the arithmetic will transform, in which the GLCM properties and HF surface signifies that the attribute rate of the surface relies on the number of scales in the quantized picture, which is mathematically expressed as

$$H = \sum_{i=a}^{A} \sum_{j=b}^{B} \varphi(i, j, g(P)) \psi(p(i, j)) \tag{3}$$

where ψ is referred to as an element function of P, g is signified as a vector-valued function of P, i and j represent the gray levels being compared and ϕ is referred to as an indices function.

Here,

$$a = b = 1,$$

$$A = B = N\ (desired\ number\ of\ gray - levels)$$

$$g(P) = (\mu_x, \mu_y, \sigma_x, \sigma_y),\ \psi(p(i,j)) = p(i,j),$$

$$\phi(i, j, g(P)) = \left(\frac{i-\mu_x}{\sigma_x}\right)\left(\frac{j-\mu_y}{\sigma_y}\right)$$

$$H = \sum_{i=1}^{N}\sum_{j=1}^{N}\left(\frac{i-\mu_x}{\sigma_x}\right)\left(\frac{j-\mu_y}{\sigma_y}\right)p(i,j)$$

E. Local ternary pattern (LTP)

It has been identified in previous research that the descriptions from Local Binary Patterns (LBP) commonly offer huge-discerning attributes for the categorization of barks. However, several issues such as revolution and noise vulnerability as well as automation difficulty were their major drawbacks. Thus, the LTP pattern is introduced as a surface description that removes huge-discerning attributes. LTP can resist revolution and noise and is also vigorous to inclination, in which every picture element of imagery has an LTP which is enumerated with a 1,0,1 code, and is articulated with the following expression

$$LTP_{P,R} = \sum_{i=0}^{i-1} s(g_i - g_c)3^i \quad (4)$$

where, g is referred to as the user threshold for coding. i is the index of the neighbor pixel in a predefined order. The result of the $LTP_{P,R}$ accelerator for every picture element of imagery is a P-bit binary numerical with 3P varied values which improve the calculation difficulty with minimalism and reduction of mathematical difficulty.

F. Scale-invariant feature transform (SIFT)

The SIFT is considered as an image description for the imagery-based similarity, which is constant to conversions, revolutions, and alterations within the image area and vigorous to the average transmission of perception as well as clarification difference.

Analytically, the SIFT has been stated to be beneficial in the training for the similarity of imagery and identification of the objectives beneath the physical situations.

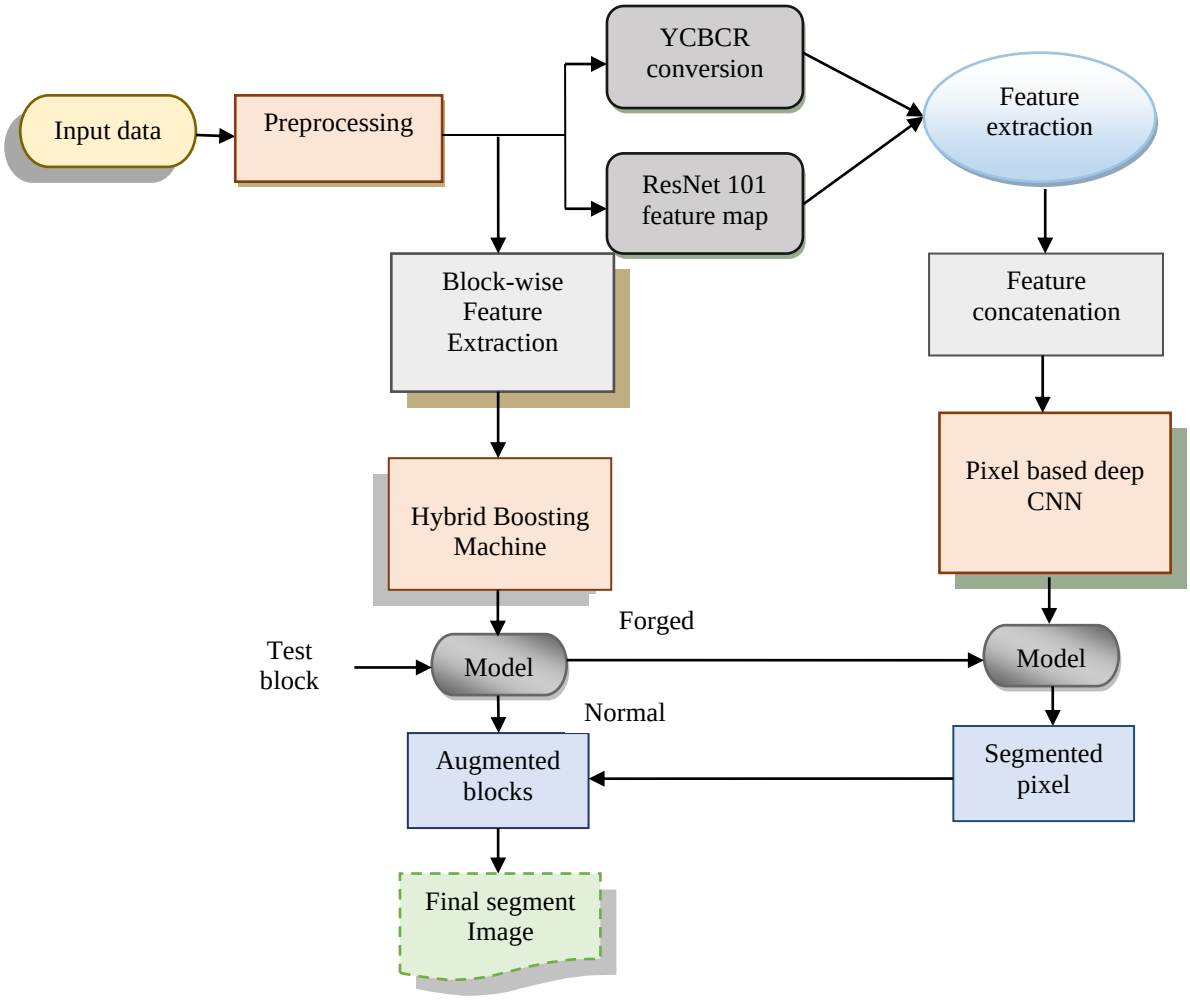

Fig.1.Systematic presentation of Proposed Method

The technique for identifying the interesting spots in the SIFT mechanism can be viewed as a differentiation of the identification of the scale-adaptive blob technique based on convolution along with Gaussian kernels and is articulated as

$$G(a,b,s)=\frac{1}{2\pi S}e^{-(a^2+b^2)/(2s)} \tag{5}$$

where (a,b,s) is denoted as the input values, S is specified as the variance of the Gaussian kernel.

G. Light coefficient features

The light coefficients are calculated in a block-wise manner; the summation of the absorption and the coefficient dispersion of light is intended. At present, it is unclear which portion of optical attenuation could be qualified to the light dispersion and which to absorption. Therefore, few publications are concerned merely with light absorption. Nevertheless, considering the huge amount of defects, the light dispersion could additionally create an extensive contribution to the totality reduction of light, which is expressed mathematically as

$$I_{cf}=\frac{3}{16\pi}\cos^2\theta \tag{6}$$

where, I_{cf} is referred to as the Light coefficient features.

H. Hybrid Boosting Machine

The Hybrid Boosting Machine describes a common structure for boosting a guideline technique, like the standard logistic regression technique. For boosting the guideline method, non-linear techniques such as random forests (RF), XGBoost, extreme learning machines, or integrated methods could be implemented. For example, the RF or XGBoost methods can be implemented to evaluate the importance of the features as well as to detect the extra variables that are utilized to enhance the calculation. The boosting technique is based on the augmented family distribution utilized in the generalized linear methods, in which an arbitrary variable Y belongs to the augmented family distribution if the mass allocation can be articulated as

$$\log f_a(a/\theta,\phi)=\frac{a\theta-v(\theta)}{u(\phi)}+w(a,\phi) \tag{7}$$

where θ is referred to as the canonical parameter, ϕ is defined as the dispersion parameter, as well as $v(\theta)$, $w(a,\phi)$, and $u(\varphi)$ were the functions correlated to the mass distribution of a. Based on the Eq. (7), the log-likelihood function can be articulated as

$$\log lik=\sum_{i=1}^{M}\frac{a_i\theta_i-v(\theta_i)}{u(\phi)}+w(a_i,\phi) \tag{8}$$

The current rejoinder of the boosted guide-line method is expressed as

$$\widehat{P}(A=1)=e^{\theta_i(b_i)}/(1+e^{\theta_i(b_i)}) \tag{9}$$

In every latest measure $(m\geq 2)$ of the boosting algorithm, current pseudo retaliations are produced based on the variations among experimental as well as accumulated responses of traditional layers of the methods. Thus, every current pseudo-retaliation holds details that are not captured by previous layers. For the regression issues, the boosting algorithm generates consecutive layers of methods by utilizing the remainder of the traditional layers as fresh pseudo-retaliations for the impending layers.

I. Segmentation Model

The pre-processed input data is further subjected to the process of segmentation with YCBCR conversion as well as the ResNet 101 feature map which is described briefly in this section.

a. YCBCR conversion

The color-space alternation is one of the significant changes in the image processing executions, in which the live images, and recordings, are saved in the color space of RGB (red, green, and blue), as it is based on the color vulnerability identification cells in the human vision network. Moreover, in virtual functioning, the YCbCr color space is frequently used to utilize the lesser declaration potential of the human vision network for color concerning brightness. Therefore, the RGB to YCBCR alternation is extensively utilized in the processing of images as well as video, which is attained based on the expression

$$YCBCR=rgb2ycbcr(RGB) \tag{10}$$

b. ResNet 101 Feature map

The highly developed VGG-19 approach, which addresses both object identification and image categorization, serves as the inspiration for the ResNets-101 plan. Typically, a CNN technique consists of a few layers that are both specialized for different tasks and related to one another. At the end of the layering process, the system learns different attribute scales. The size of the convolutional layers in this technique consists primarily of 33 filters, and each layer contains a similar number of filters for a similar feature map outcome range. The amount of filters is increased when the feature map volume is reduced halfway, which helps to manage the time complexity of each layer and exposes down sampling by convolutional layers with double strides. Moreover, the ResNet-101 concludes with an inclusive average layer of pooling and a SoftMax-activated completely related layer. The module of ResNet-101 is demonstrated in Fig.2.

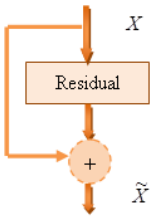

Fig.2.ResNet-101 Module

J. Feature Concatenation

The input images and their features which are converted based on the YCBCR, as well as the ResNet 101 feature map, are further subjected to feature concatenation to

combine them with varied depths and structures for the accomplishment of better segmentation accuracy.

K. Pixel-based deep CNN

The optimized DCNN consists of pooling, contortion, fully connected, and SoftMax functionality. It is advanced by an added layer that utilizes an attribute tensor and the 180*16 shape, where 180 represents each sensor's sequential aspect and 16 represents the number of sensors. Additionally, there is a traditional layer with thirty-two kernels, all of which have 2×1 ranges, 1×1 strides, comparable padding, and a ReLU activation process that is used to extract effective and outstanding attribute characteristics. In addition, a high layer of pooling with a 2×1 range and 1×1 stride is used to shorten each sensor's sequential data length. Except for the number of kernels alternating by 16, the binary layer of convolutional and the high layer of pooling are comparable to the traditional layers. The data matrix then became 45×16. The last three convolutional layers resemble the binary layer. After that, there is a completely related layer with over a thousand nodes and the SoftMax layer with roughly ten nodes, also known as ten dendrobium kinds. In this case, the optimized DCNN is suitable for the E-nose because the involution kernel's range remains constant when paired with the E-nose's data. Furthermore, each picture element in an image is connected to its neighboring picture elements for the image to function. To eliminate educational features, the square of 2D kernels is used. This differs from the image functioning where the sensors were self-regulating even if the sequential aspect is connected. As a result, the lined 1D convolutional kernels are used for more than just eliminating inefficient characteristics; they also keep track of the feature justifications for the added images. Additionally, the neurons in the convolutional layers were organized into feature maps. These feature maps have an accessible sector that is linked to neuron regions in the preceding layer through the use of a skillful pair of weights that are periodically displayed as a filtered stock. The inputs of this feature map are associated with the mass that was previously trained to measure it, and the convoluted outputs are transmitted through a nonlinear process of activation that is expressed arithmetically as

$$X_e = f(FM_e^* I_m^{seg}) \tag{11}$$

where X_e is defined as the output feature map, I_m^{seg} is defined as the input image, and FM_e^* is referred to as the feature map connected with the convolutional filter.

The forged input image gathered from the classification process then gets subjected to the proposed technique in the segmentation process, in which the model combines and masks the forged image, which is then fed forward to the segmented pixel. The segmented pixel is the process of highlighting the pixels in an image that are forged and passing them to the augmented blocks. The augmented blocks are classified into the finished blocks and unfinished blocks for the test genotypes. In a randomized finished block pattern, tests are simulated similarly in every block, whereas in the unfinished block design, the block volumes are different, which produces the desired final segment image.

IV. Results and Discussion

The result attained through the image splicing detection by utilizing the Hybrid Boosting Machine model is established in the subsequent section.

A. Experimental setup

The experiment is executed in PYTHON, which provides instance-efficient and ordered programming. The implementation system includes PyCham software and is implemented in the Operating system of Windows 10 with 8GB RAM as memory.

B. Datasets

The input data is collected from the standard DTS such as DSO-1 and DSI-1 [14], in which DSO-1 is collection of 200 interiors as well as outside images with an image assertion of 2,048 x 1,536 picture elements, and DSI-1 is collection of 50 images and are downloaded from various sites in the internet with various resolution.

C. Experimental Analysis

The image results acquired from the experiment based on the datasets [14] have been demonstrated in this section in terms of original and output images as well as the results obtained from the ResNet Feature Map and YCBCR conversion have also been represented in Fig.3 and Fig.4.

D. Performance Metrics

a) Accuracy

The accuracy is evaluated as the degree of approximation to the target value of the detection and represented as,

$$Acc = \frac{n^{ca}}{n^{a}} \tag{12}$$

where, n^{ca} is specified as the number of correct analyses, as well as n^{a} is recognized as the whole number of analyses.

b) Sensitivity

The sensitivity is evaluated on account of the positive instances recognized by the existing approaches together with the gathered DTS by utilizing the below expression

$$SN = \frac{t_p}{t_p + t_n} \tag{13}$$

where, t_p is defined as the true positive as well as t_n is referred to as the true negative.

c) Specificity

The specificity is evaluated concerning the fraction of true negatives to the overall negatives with the given expression

$$S_p = \frac{t_n}{t_n + t_p} \tag{14}$$

where t_n is specified as the true negative and t_p is referred to as the true positive.

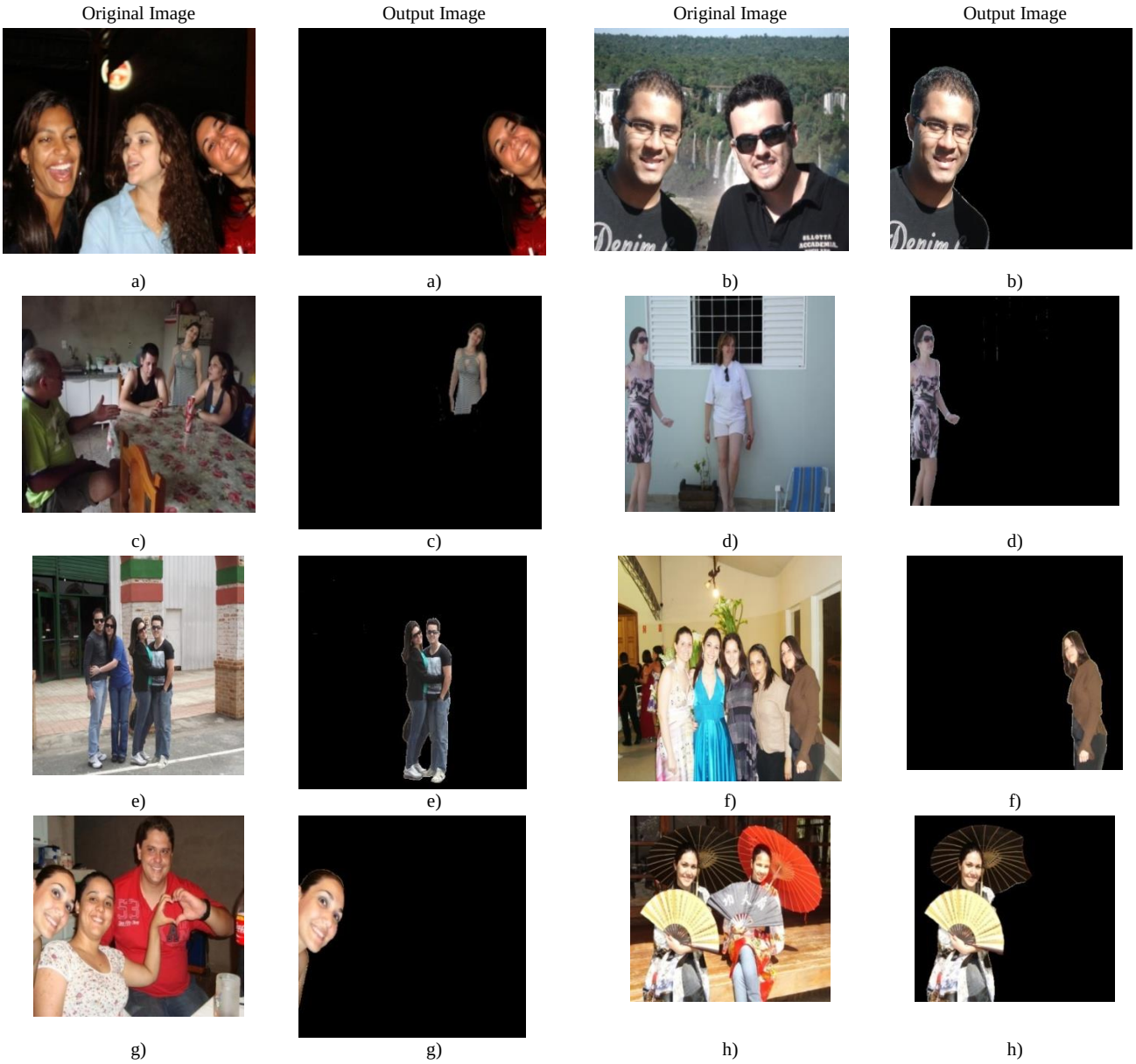

Fig.3. Experimental outcome based on the dataset DSO-1 and DSI-1

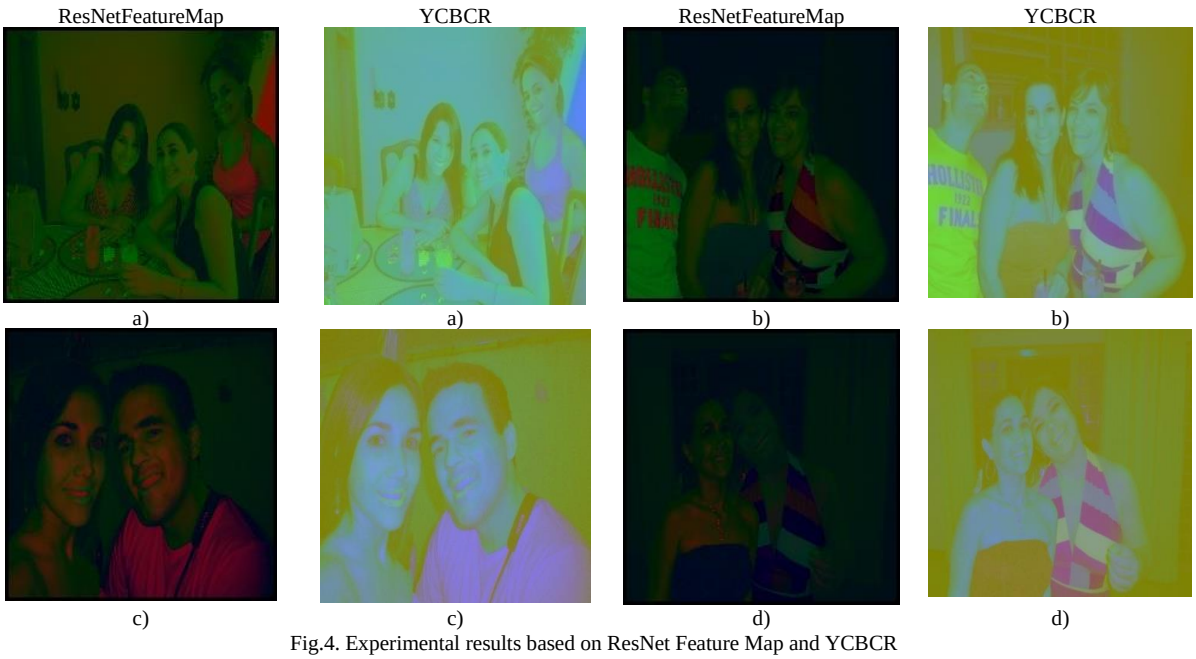

Fig.4. Experimental results based on ResNet Feature Map and YCBCR

d) Mean square error (MSE)
The MSE measures the average squared difference between the predicted and actual values. A lower MSE signifies better model performance, indicating that the model's predictions are closer to the true values.

$$MSE = \frac{1}{n}\sum_{i=1}^{n}(S_i - \hat{S}_i)^2 \quad (15)$$

Where n is the number of samples, S_i is the real value and $\hat{S}_i$ is the predicted value.

E. Performance Analysis

This section depicts the performance of the Hybrid Boosting Machine to obtain the detection of image splicing by utilizing metrics concerning the DTS [14].

Performance evaluation concerning the Training Percentage (TP) on the DSO-1

The performance evaluation of the Hybrid Boosting Machine is evaluated by utilizing the dataset DSO-1 [14] particularly, concerning metrics such as accuracy, sensitivity, and specificity.
Table I shows the accuracy, Table II shows sensitivity and Table III shows specificity of the model with TPs from 40% to 90% and epochs from 100 to 300.
Fig.5 depicts the performance evaluation of the Hybrid Boosting Machine model on DSO-1 at TP 90% for epochs 100 to 300.

Table I. Hybrid Boosting Machine Accuracy on DSO-1

Training Percentage	No. of Epochs				
	100	150	200	250	300
TP-40	94.64	94.64	94.78	94.78	94.81
TP-50	94.81	94.82	94.85	94.89	94.91
TP-60	94.84	94.85	94.89	94.89	94.91
TP-70	94.86	94.87	94.9	94.9	94.97
TP-80	94.94	94.94	94.96	94.99	95.03
TP-90	95.04	95.12	95.12	95.12	95.19

Table II. Hybrid Boosting Machine Sensitivity on DSO-1

Training Percentage	No. of Epochs				
	100	150	200	250	300
TP-40	94.06	94.08	94.19	94.22	94.22
TP-50	94.22	94.23	94.26	94.29	94.34
TP-60	94.23	94.25	94.28	94.31	94.36
TP-70	94.25	94.30	94.31	94.32	94.36
TP-80	94.29	94.32	94.34	94.38	94.38
TP-90	94.37	94.39	94.39	94.43	94.48

Table III. Hybrid Boosting Machine Specificity on DSO-1

Training Percentage	No. of Epochs				
	100	150	200	250	300
TP-40	95.06	95.08	95.15	95.16	95.17
TP-50	95.11	95.19	95.28	95.35	95.39
TP-60	95.28	95.32	95.36	95.41	95.44
TP-70	95.33	95.41	95.44	95.45	95.58
TP-80	95.45	95.51	95.52	95.59	95.65
TP-90	95.47	95.61	95.65	95.80	95.87

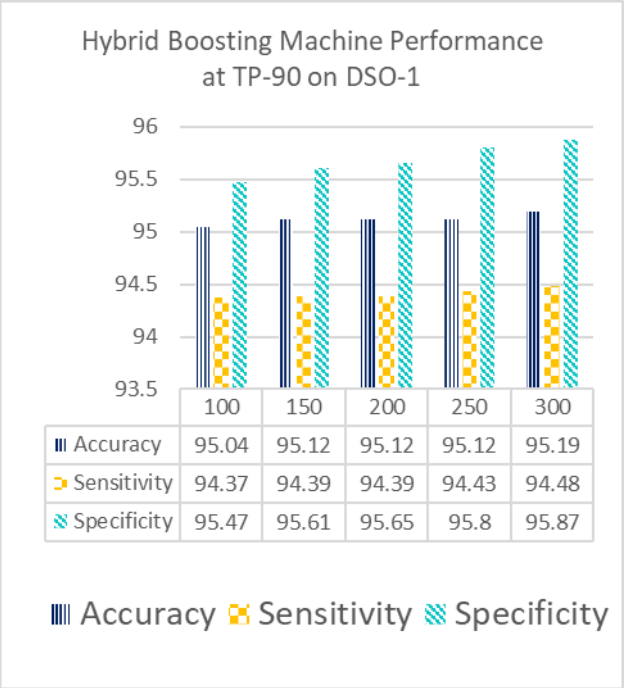

Fig.5. Performance evaluation of the Hybrid Boosting Machine model on DSO-1

Performance evaluation concerning the TP on DSI-1

The performance evaluation of the Hybrid Boosting Machine is evaluated by utilizing the dataset DSI-1 [14] particularly, concerning metrics such as accuracy, sensitivity, and specificity.
Table IV shows the accuracy, Table V shows sensitivity and Table VI shows specificity of the model with TPs from 40% to 90% and epochs from 100 to 300.
Fig.6 depicts the performance evaluation of the Hybrid Boosting Machine model on DSI-1 at TP 90% for epochs 100 to 300.

Table IV. Hybrid Boosting Machine Accuracy on DSI-1

Training Percentage	No. of Epochs				
	100	150	200	250	300
TP-40	90.65	90.69	90.75	90.92	91.15
TP-50	90.85	91.25	91.28	91.58	91.94
TP-60	91.45	91.83	92.10	92.19	92.19
TP-70	91.55	92.24	92.41	92.41	92.70
TP-80	92.41	92.57	93.02	93.19	93.23
TP-90	94.28	94.33	94.33	94.61	94.78

Table V. Hybrid Boosting Machine Sensitivity on DSI-1

Training Percentage	No. of Epochs				
	100	150	200	250	300
TP-40	89.25	89.75	90.00	90.00	90.11
TP-50	89.85	90.17	90.22	90.45	90.64
TP-60	90.35	90.35	90.64	90.99	91.65
TP-70	90.69	90.92	91.51	92.37	92.66
TP-80	92.52	93.11	93.21	93.50	93.50
TP-90	93.27	93.86	94.01	95.29	95.39

Table VI. Hybrid Boosting Machine Specificity on DSI-1

Training Percentage	No. of Epochs				
	100	150	200	250	300
TP-40	90.34	90.42	90.44	90.68	90.90
TP-50	90.61	90.87	90.95	91.20	91.61
TP-60	91.21	91.45	91.73	91.94	92.07
TP-70	91.32	92.02	92.07	92.14	92.46
TP-80	92.19	92.20	92.90	93.02	93.08
TP-90	94.02	94.09	94.12	94.38	94.54

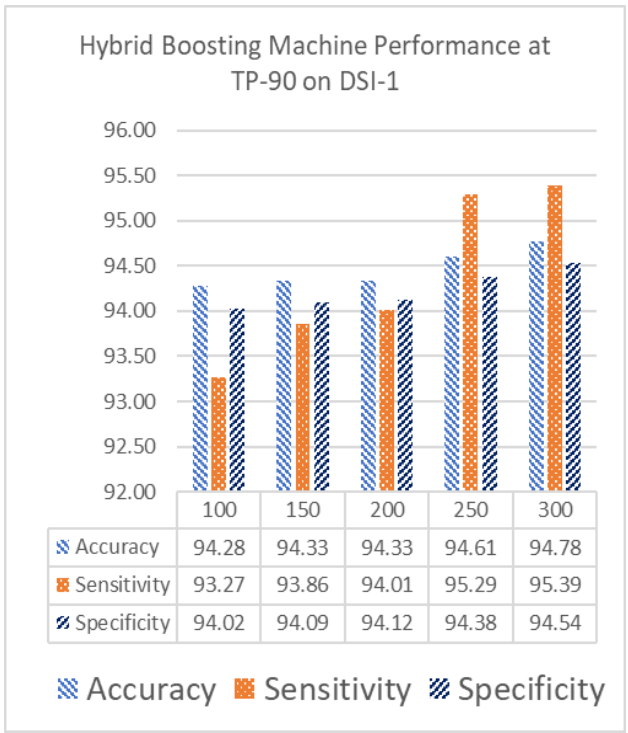

Fig.6. Performance evaluation of the Hybrid Boosting Machine model on DSI-1

F. Comparative evaluation

The comparative evaluation of the Hybrid Boosting Machine approach is evaluated with a few traditional techniques such as Linear Regression (LR) classifier (MD_1), DeepCNN (MD_2), SVM (MD_3), Decision Tree (DT) (MD_4), and Naïve Bayes (NB) (MD_5).

Comparative evaluation utilizing the TP on DSO-1

The comparative evaluation is conducted on the DTS DSO-1 [14] and the results are obtained based on accuracy, sensitivity, specificity, and ROC/AUC.
The accuracy of the Hybrid Boosting Machine method established by TP 90 with epoch 300 is 94.74%, which is an improvement of 52.08% over MD_1, 20.50% over MD_2, 8.89% over MD_3, 0.64% over MD_4, and 0.28% over MD_5. However, the Hybrid Boosting Machine method's sensitivity at TP 90 with epoch 300 is 95.00%, an improvement over the preceding technique MD_1, 23.92% from MD_2, 10.92% from MD_3, 0.66% from MD_3, and 0.25% from MD_5. At TP 90, the specificity value of the Hybrid Boosting Machine technique with epoch 300 is 95.27%, which is improved from 16.03% in the current MD1, 15.50% in the MD2, 15.28% in the MD3, 11.59% in the MD4, and 8.57% in the MD5, respectively. The ROC of the Hybrid Boosting Machine model achieves 0.833, 0.867, 0.883, 0.910, 0.917, 0.918, 0.922, 0.943, and 0.947, which are higher than the other existing techniques such as MD_1, MD_2, MD_3, MD_4, and MD_5.The Hybrid Boosting Machine method attains an MSE of 3.18 which is very much less than other existing methods attaining 11.97, 6.77, 5.77, 4.25, and 4.16 for MD_1, MD_2, MD_3, MD_4, and MD_5 respectively.
The systematic representation of the comparative analysis is depicted in Fig.7.

The analysis revealed that the performance of the Hybrid Boosting Machine outperformed the existing techniques

Comparative analysis concerning the TP on DSI-1

The comparative analysis is performed according to the DTS DSI-1 [14] and the result is achieved in terms of accuracy, sensitivity, specificity, and ROC/AUC. The accuracy of the Hybrid Boosting Machine approach at TP 90 with epoch 300 is 94.86%, which is improved by 12.29% compared to the MD_1, 9.53% compared to MD_2, 9.18% compared to MD_3, 6.22% compared to MD_4, and 2.29% compared to MD_5. However, the Hybrid Boosting Machine approach's sensitivity at TP 90 with epoch 300 is 94.97%, which is an improvement over the MD_1, 37.64% to MD_2, 29.57% to MD_3, 22.38% to MD_4, and 18.73% to MD_5. At TP 90, the specificity of the Hybrid Boosting Machine approach with epoch 300 is 93.38%, up 23.31% from the MD_1, 22.20% from MD_2, 18.47% from MD_3, 17.34% from MD_4, and 15.11% from MD_5, correspondingly. The ROC of the Hybrid Boosting Machine model attains 0.829, 0.861, 0.880, 0.904, 0.913, 0.916, 0.920, 0.933, and 0.945, which are higher than the other existing techniques such as MD_1, MD_2, MD_3, MD_4, and MD_5. The Hybrid Boosting Machine method attains an MSE of 5.29 which is very much less than other existing methods attaining 13.36, 11.59, 6.89, 5.52, and 5.47 for MD_1, MD_2, MD_3, MD_4, and MD_5 respectively.

The analysis proves that the Hybrid Boosting Machine model outperformed the existing techniques. The systematic demonstration of the comparative evaluation is shown in Fig.8.

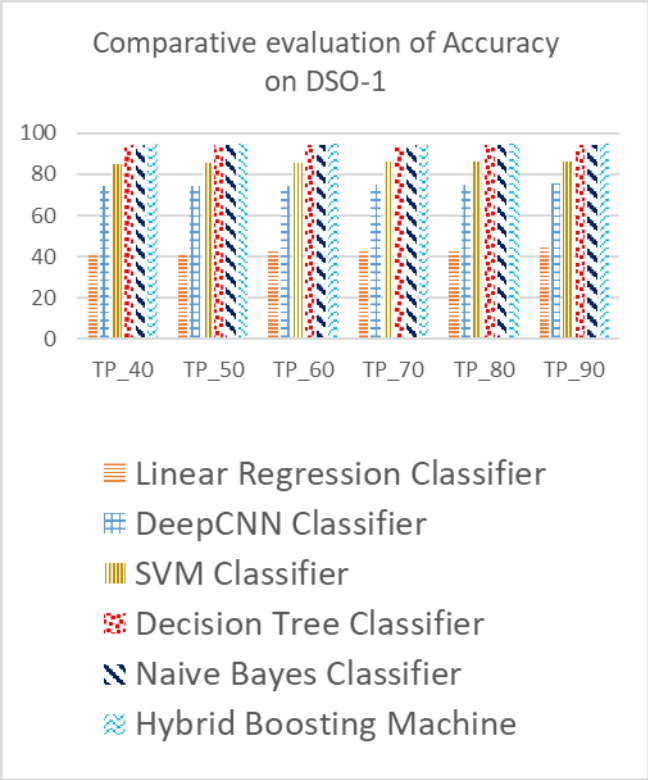

a) Accuracy

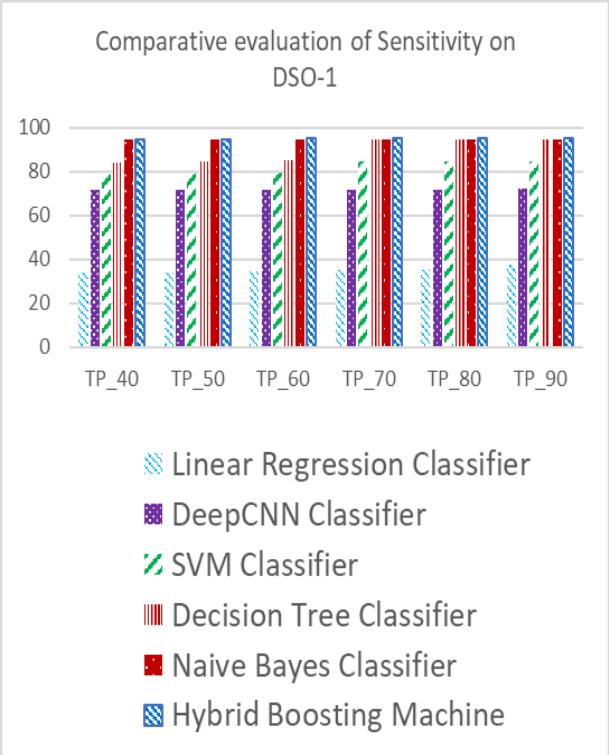

b) Sensitivity

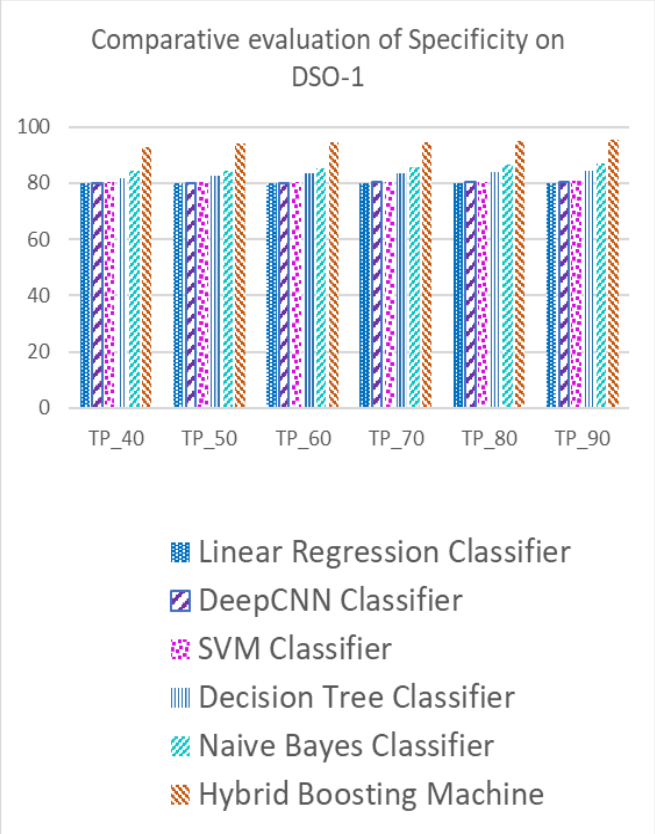

c) Specificity

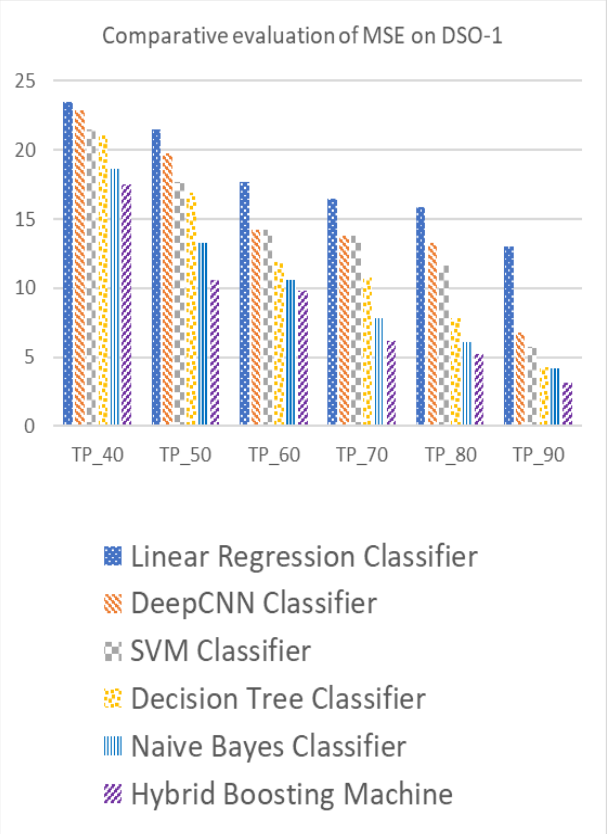

d) MSE

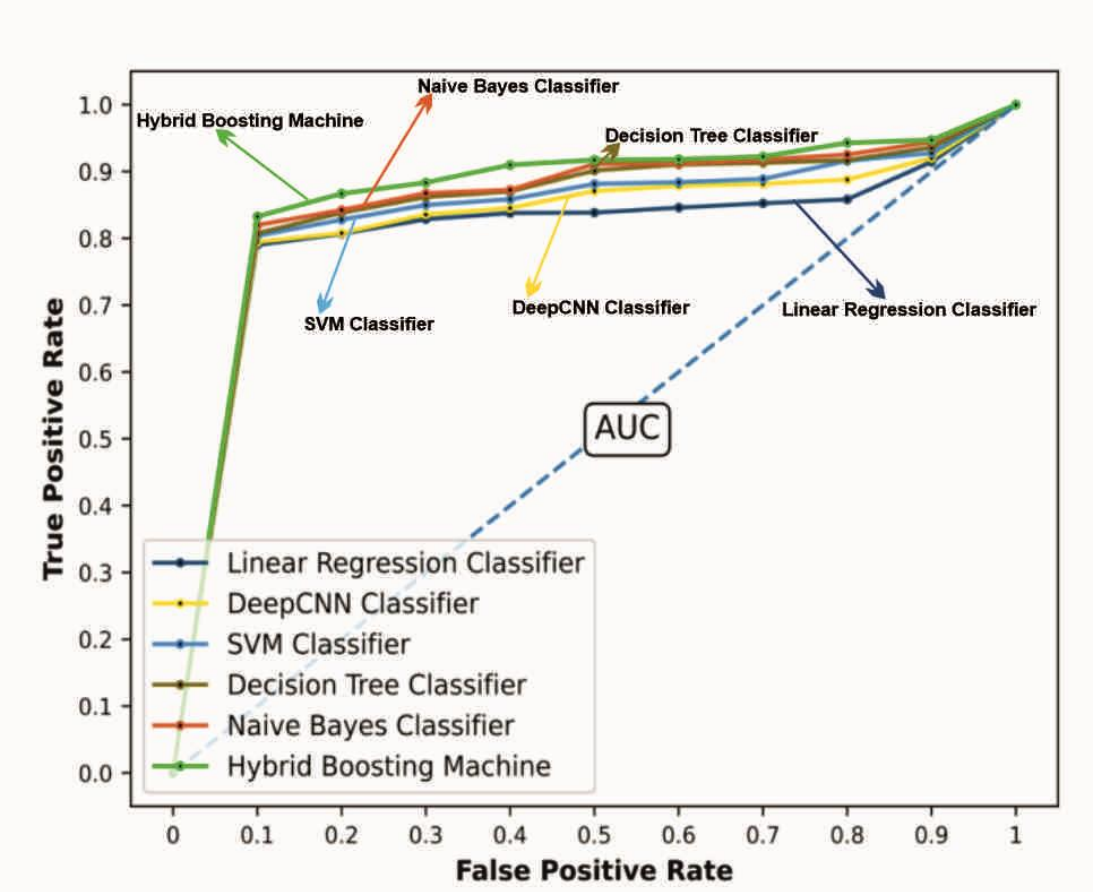

e) ROC/AUC Curve

Fig.7.Comparative evaluation of the proposed method based on the DSO-1 a) Accuracy b) Sensitivity c) Specificity d) MSE and e) ROC/AUC Curve

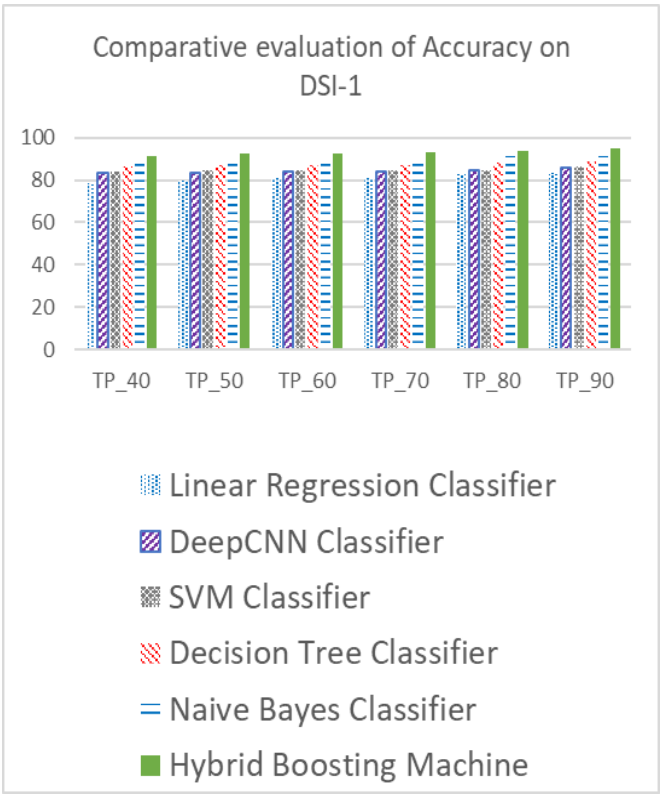

a) Accuracy

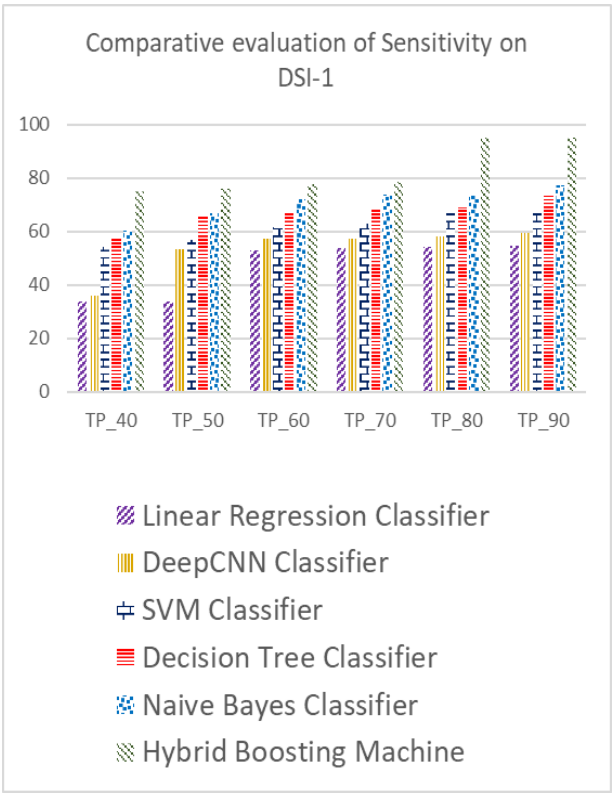

b) Sensitivity

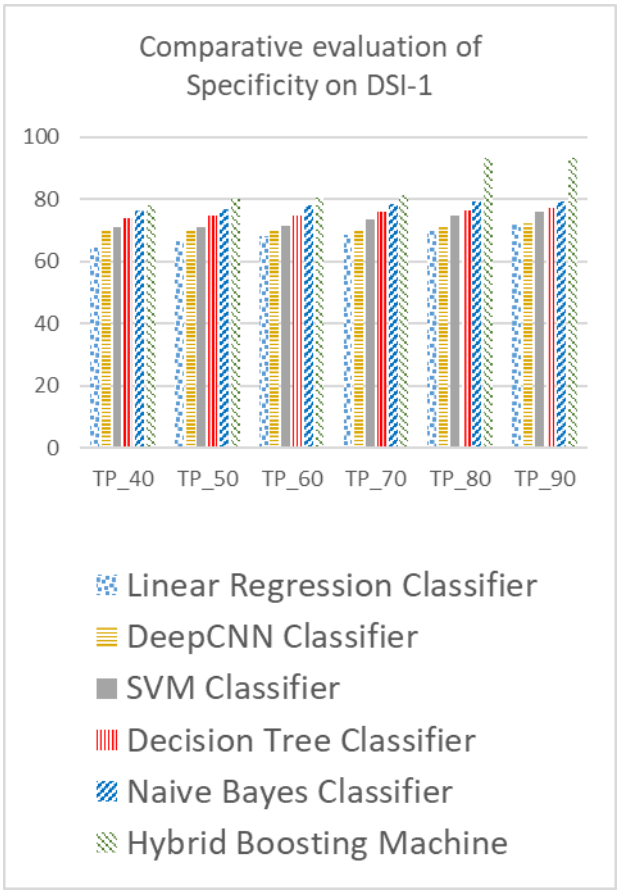

c) Specificity

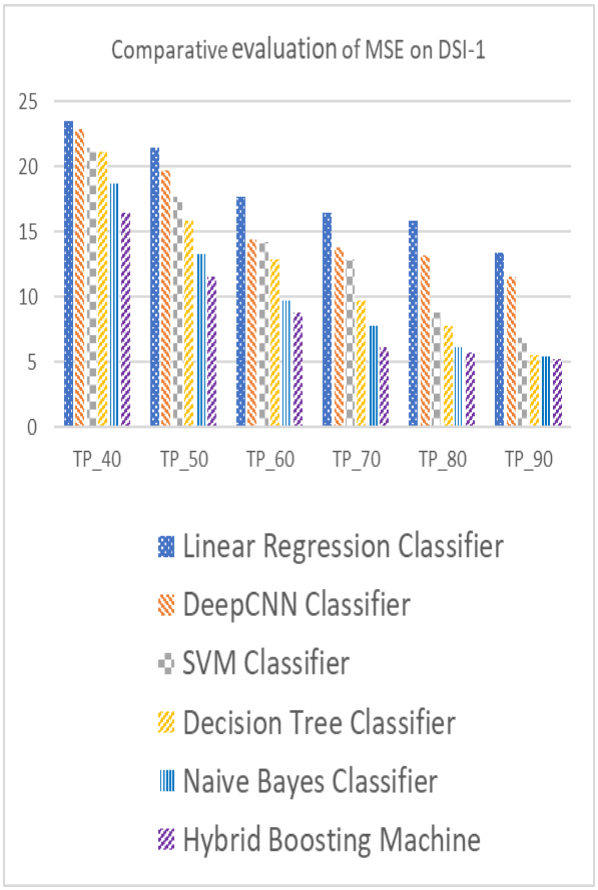

d) MSE

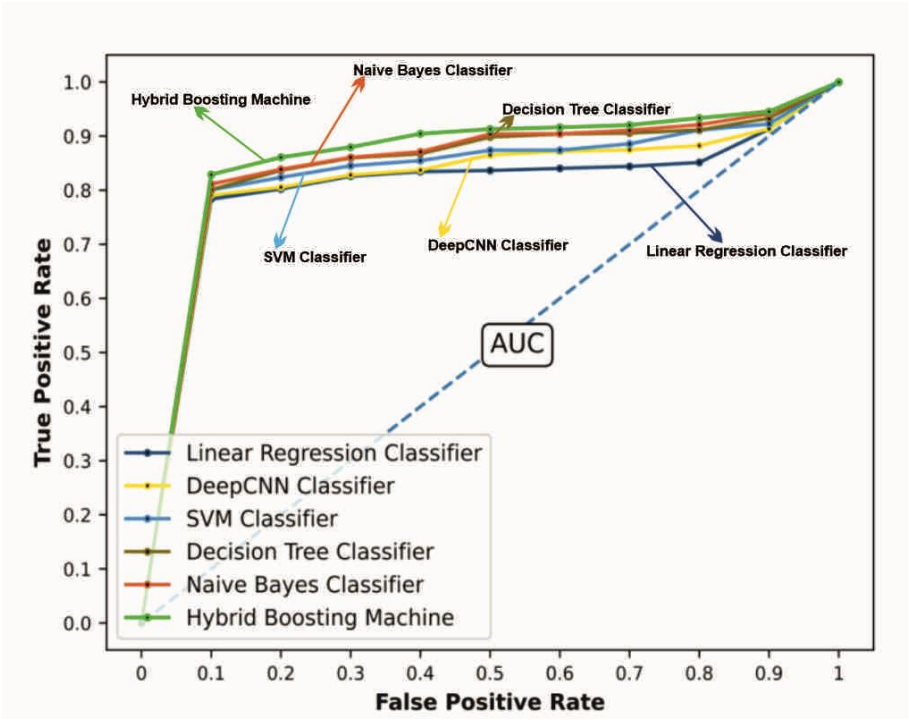

e) ROC/AUC Curve

Fig.8.Comparative evaluation of the proposed method based on the DSI-1 a) Accuracy b) Sensitivity c) Specificity d) MSE and e) ROC/AUC Curve

Comparative evaluation concerning the K-Fold on DSO-1

The comparative evaluation concerning the k-fold utilizing the DSO-1 dataset is performed for the Hybrid Boosting Machine model, in which different metrics are evaluated and are illustrated in Fig.9. The accuracy of the Hybrid Boosting Machine at k-fold 10 is 95.145% which shows 18.82% improvement over the existing LR technique, 10.23 % over

Deep CNN,6.30% over SVM,4.65% over DT, and 1.67% over the NB technique. The sensitivity of the Hybrid Boosting Machine model at k-fold 10 is 95.63% which shows 33.81 % improvement over the existing LR technique, 24.77 % over Deep CNN, 22.26 % over SVM, 17.37 % over DT, and 4.95% over NB technique. Further, the specificity of the Hybrid Boosting Machine at k-fold 10 is 94.76% which shows 22.56% improvement over the existing LR technique, 11.96 % over Deep CNN, 9.56 % over SVM, 6.70 % over DT, and 2.22 % over NB technique. The analysis revealed that the Hybrid Boosting Machine model surpassed the other existing techniques.

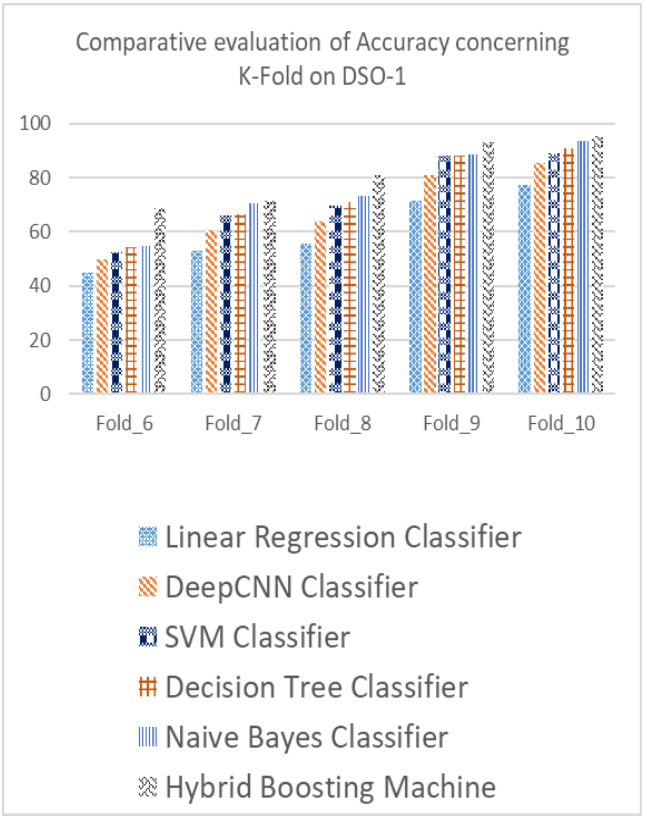

a) Accuracy

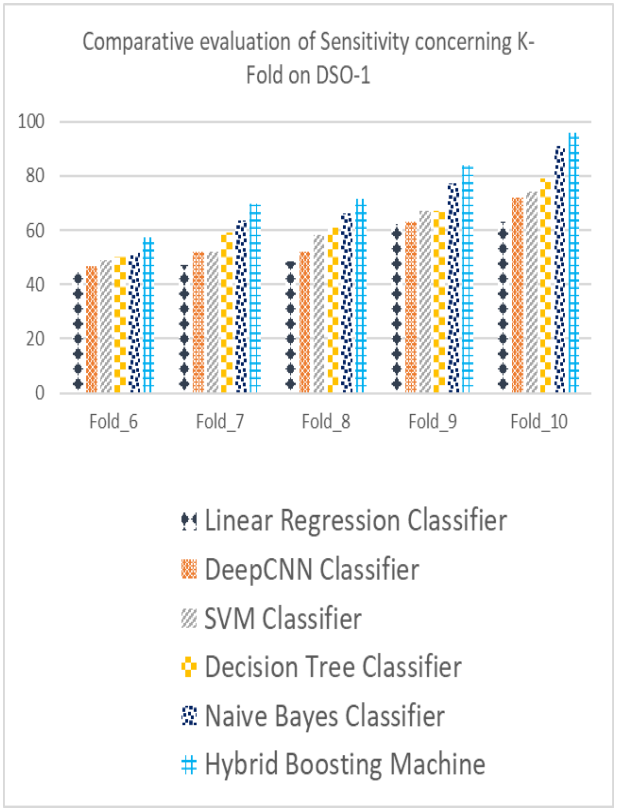

b) Sensitivity

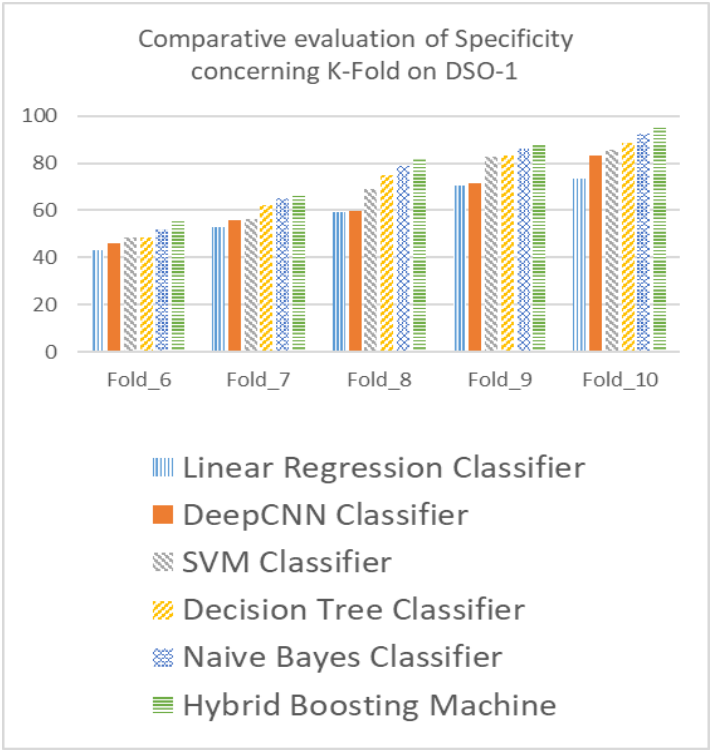

c) Specificity

Fig.9. Comparative evaluation concerning the K-Fold on DSO-1a) Accuracy b) Sensitivity c) Specificity

Comparative evaluation utilizing the K-Fold on DSI-1

The comparative analysis utilizing the k-fold utilizing the DSI-1 dataset was performed for the Hybrid Boosting Machine model, in which different metrics are evaluated and are depicted in Fig.10. The accuracy of the Hybrid Boosting Machine model at k-fold 10 is 95.59% which shows 9.37% improvement over the existing LR technique, 5.37% over Deep CNN, 2.78% over SVM, 0.52% over DT, and 0.22% over NB technique. The sensitivity of the Hybrid Boosting Machine model at k-fold 10 is 94.26% which shows 4.65% improvement over the existing LR technique, 3.43% over Deep CNN, 2.77% over SVM, 1.33 % over DT, and 1.13% over NB technique. Further, the specificity of the Hybrid Boosting Machine model at k-fold 10 is 95.59% which shows 6.55% improvement over the existing LR technique, 2.87% over Deep CNN, 2.17% over SVM, 1.61 % over DT and 1.02 % over NB technique. The analysis revealed that the Hybrid Boosting Machine model surpassed the other existing techniques.

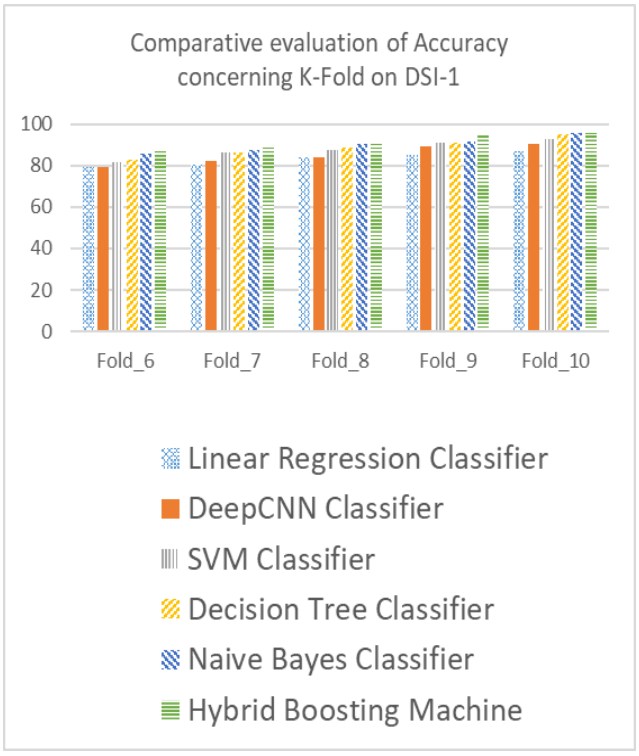

a) Accuracy

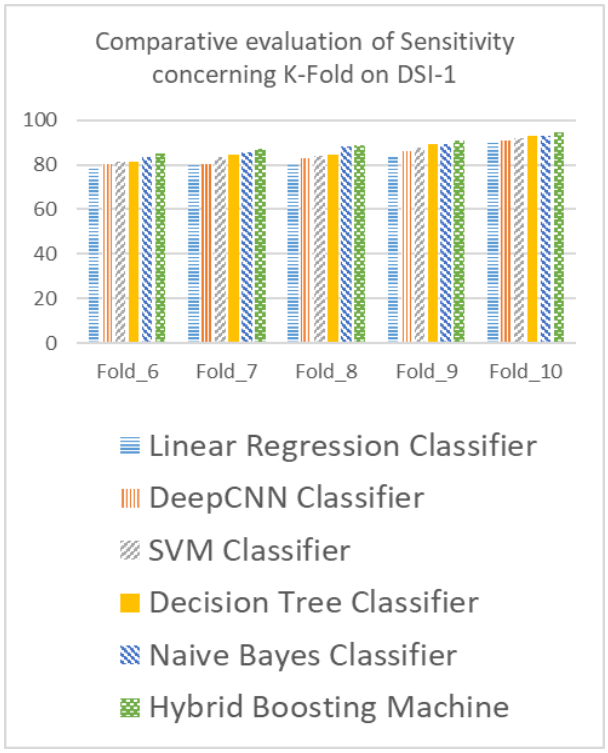

b) Sensitivity

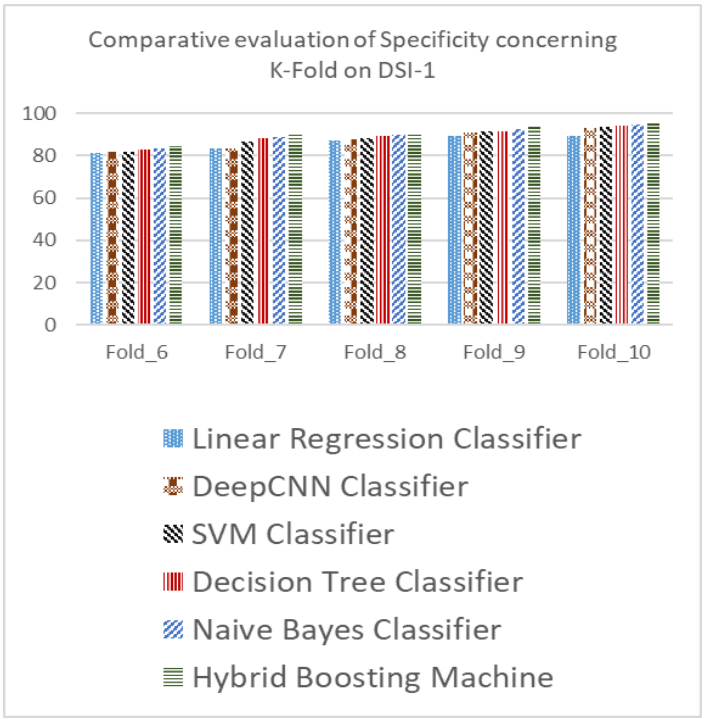

c) Specificity

Fig.10. Comparative evaluation concerning the K-Fold on DSI-1 a) Accuracy b) Sensitivity c) Specificity

V. Comparative Discussion

The comparative discussion of the Hybrid Boosting Machine approach and existing techniques is displayed in Table VII.

This section provides a quick overview of the analysis of the effects of various image forgery detection methods. The existing techniques such as LR classifier, DeepCNN, SVM, Decision Tree (DT), and Naïve Bayes (NB) have some limitations in effectively performing image forgery detection. The Deep CNN model [16] detected only whether an image is spliced or not, but does not localize the sliced regions in images that forms the limitation. The drawback of LR model is that positive outcomes are not obtained [15]. The SVM model does not perform well on images with more noise and requires optimization techniques to enhance the performance [17]. Further, the DT technique attained limited accuracy [18]. The NB model was found with computational complexity that limited the performance [19]. However, the proposed method overcame the above limitations by utilizing the block-wise feature extraction and a Hybrid Boosting Machine segmentation approach that enhanced the detection accuracy. Based on this comprehensive comparative analysis, it is evident that the Proposed Hybrid Boosting Machine is the superior choice for Image forgery detection from both the DSO-1 and DSI-1 datasets, offering a robust and balanced solution for a wide range of applications.

Comparative analysis includes LR, Deep-CNN, SVM, DT, and NB classifiers. The DSO-1 and DSI-1 databases are used for the comparative analysis, which shows how well the classifiers perform at the early computation stage of image forgery detection. The Hybrid Boosting Machine model is the most promising method when compared to other classification techniques using the DTS DSO-1 and DSI-1 datasets. The Hybrid Boosting Machine constantly outperforms conventional methods like LR, Deep-CNN, SVM, DT, and NB classifiers when measured on a variety of criteria.

Against all other approaches, it outperforms with outstanding accuracy of 94.74% for DSO-1 and 94.86% for DSI-1. It also performs exceptionally well in terms of sensitivity and specificity, ensuring a balanced prediction capacity; its respective values are 95.00% and 95.27% for DSO-1 and 94.97% and 93.38% for DSI-1. Also, the method shows MSE of 3.19 on DSO-1 and 5.29 on DSI-1.

To summarize, Table VII shows that the Hybrid Boosting Machine regularly outperforms other Deep Learning (DL) classifiers in terms of MSE, accuracy, sensitivity, and, most importantly, specificity on the DSO-1 and DSI-1 datasets. Because of its capacity to retain a high degree of sensitivity and specificity, it is an excellent choice for tasks where precisely identifying both positive and negative examples is essential.

VI. Statistical Analysis

The statistical analysis for dataset 1 is shown in Table VIII and the statistical analysis for Dataset 2 is presented in Table IX. Here the Hybrid Boosting Machine is compared to other existing techniques such as LR, deep-CNN, SVM, DT, and NB classifiers to show its efficiency in statistical analysis which is performed in terms of Best, Mean, and Variance for accuracy, sensitivity, and specificity.

For dataset 1, the Hybrid Boosting Machine method attains a Best of 94.72 and Mean of 94.59 for accuracy which is improved by 0.28% and 0.34% than NB respectively, and the proposed method attains a Variance of 0.005 for accuracy. As for sensitivity, the Hybrid Boosting Machine method attains a Best of 95.00 and a Mean of 94.77 which is improved by 0.25% and 0.35% than NB respectively, and the Hybrid Boosting Machine method attains a Variance of 0.08 for sensitivity. Similarly, for specificity, the Hybrid Boosting Machine method attains a Best of 95.27 and a Mean of 94.31 which is improved by 8.56% and 9.25% than NB respectively, and the Hybrid Boosting Machine method attains a Variance of 0.70 for specificity.

For dataset 2, the proposed method attains a Best of 94.86 and Mean of 93.08 for accuracy which is improved by 2.29% and 2.65% than NB respectively, and the Hybrid Boosting Machine technique attains a Variance of 0.16 for accuracy. As for sensitivity, the Hybrid Boosting Machine method attains a Best of 94.97 and a Mean of 82.85 which is improved by 18.73% and 14.72% than NB respectively, and the Hybrid Boosting Machine technique attains a Variance of 74.58 for sensitivity. Similarly, for specificity, the proposed method attains a Best of 93.37 and a Mean of 84.41 which is improved by 15.11% and 7.59% than NB respectively, and the Hybrid Boosting Machine method attains a Variance of 41.02 for specificity.

The improvement in these results for statistical analysis shows that the Hybrid Boosting Machine technique is more efficient than other existing techniques.

Table VII. Comparative discussion concerning the DTS DSO-1 and DSI-1

Methods	DSO-1 dataset				DSI-1 dataset			
	Accuracy	Sensitivity	Specificity	MSE	Accuracy	Sensitivity	Specificity	MSE
LR classifier	45.40	37.22	80.00	11.98	83.20	54.45	71.61	13.36
Deep-CNN classifier	75.32	72.27	80.50	6.77	85.82	59.22	72.65	11.59
SVM classifier	86.32	84.62	80.71	5.77	86.16	66.89	76.13	6.89
DT classifier	94.14	94.37	84.23	4.25	88.96	73.72	77.18	5.52
NB classifier	94.47	94.76	87.11	4.16	92.69	77.18	79.27	5.47
Proposed Hybrid Boosting Machine	**94.74**	**95.00**	**95.27**	**3.19**	**94.86**	**94.97**	**93.38**	**5.29**

Table VIII: Statistical Analysis for Dataset 1

Methods	Accuracy			Sensitivity			Specificity		
	Best	Mean	Variance	Best	Mean	Variance	Best	Mean	Variance
LR classifier	45.40	43.31	1.22	37.22	35.03	1.30	80.00	79.99	0.00
Deep-CNN classifier	75.32	74.73	0.10	72.27	71.77	0.06	80.50	80.22	0.03
SVM classifier	86.32	85.80	0.14	84.62	81.89	7.18	80.71	80.46	0.02
DT classifier	94.14	93.99	0.01	94.37	89.45	23.39	84.23	83.24	0.77
NB classifier	94.47	94.27	0.02	94.76	94.44	0.05	87.11	85.59	1.11
Proposed Hybrid Boosting Machine	**94.742**	**94.590**	**0.005**	**95.00**	**94.77**	**0.08**	**95.27**	**94.31**	**0.70**

Table IX: Statistical analysis for Dataset 2

Methods	Accuracy			Sensitivity			Specificity		
	Best	Mean	Variance	Best	Mean	Variance	Best	Mean	Variance
LR classifier	83.20	81.06	2.44	54.45	47.15	89.91	71.61	68.36	4.37
Deep-CNN classifier	85.82	84.31	0.54	59.22	53.42	65.84	72.65	70.64	0.89
SVM classifier	86.16	84.79	0.40	66.89	61.56	22.68	76.13	72.90	4.20
DT classifier	88.96	87.58	0.73	73.72	66.95	24.33	77.18	75.49	1.21
NB classifier	92.69	90.61	1.40	77.18	70.65	30.35	79.27	78.00	1.12
Proposed Hybrid Boosting Machine	**94.86**	**93.08**	**1.16**	**94.97**	**82.85**	**74.59**	**93.38**	**84.41**	**41.02**

Table X: Comparison of the computational time on dataset DSO-1 and DSI-1

Methods	Computational Time (seconds)	
	DSO-1	DSI-1
LR classifier	20.84	20.85
Deep-CNN classifier	20.65	20.76
SVM classifier	20.74	20.80
DT classifier	20.76	20.83
NB classifier	20.82	20.84
Proposed Hybrid Boosting Machine	**20.62**	**20.75**

Table XI: Comparison of the convergence on dataset DSO-1 and DSI-1

Methods	Error	
	DSO-1	DSI-1
LR classifier	0.19	0.36
Deep-CNN classifier	0.19	0.35
SVM classifier	0.20	0.37
DT classifier	0.19	0.36
NB classifier	0.18	0.35
Proposed Hybrid Boosting Machine	**0.17**	**0.34**

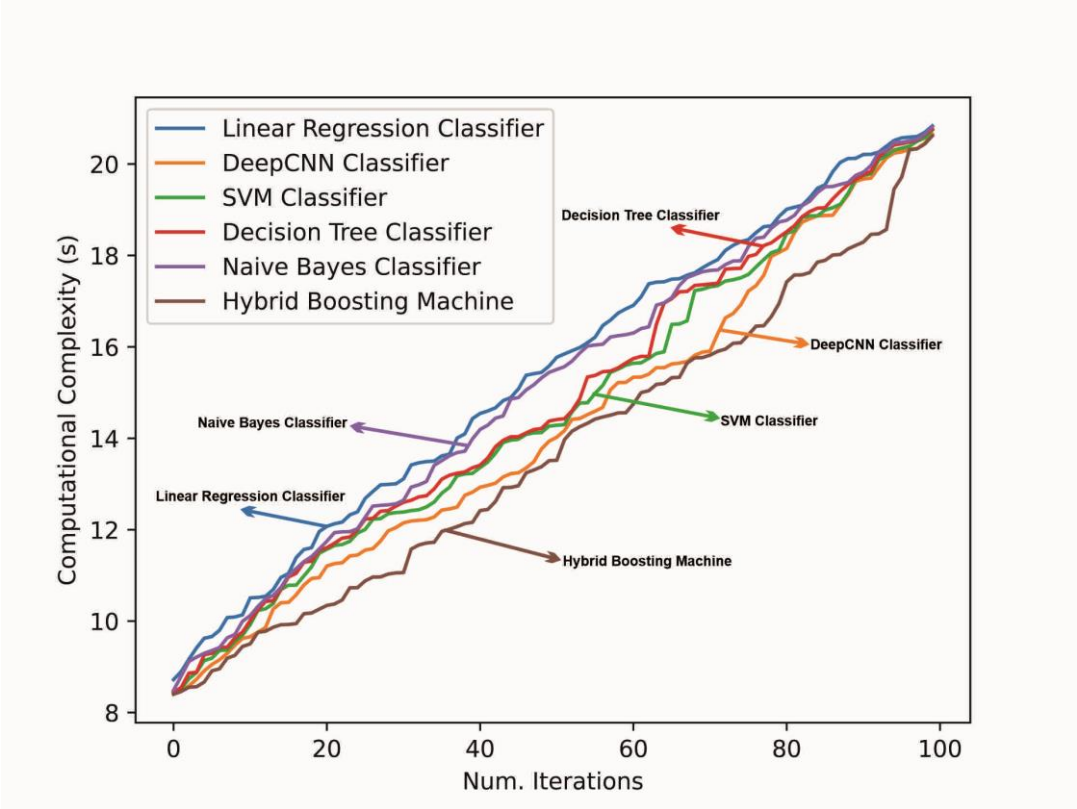

a) Time Complexity analysis on the DSO-1

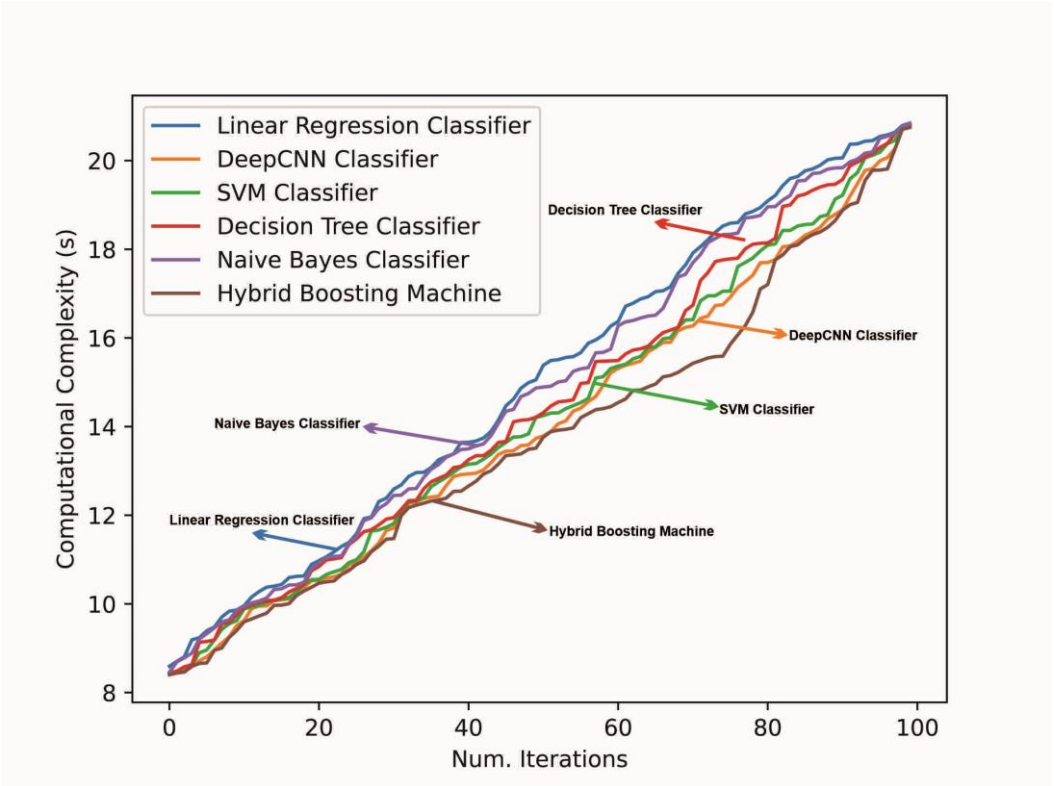

b) Time Complexity analysis on the DSI-1

Fig 11. Time Complexity Analysis of the Hybrid Boosting Machine Model

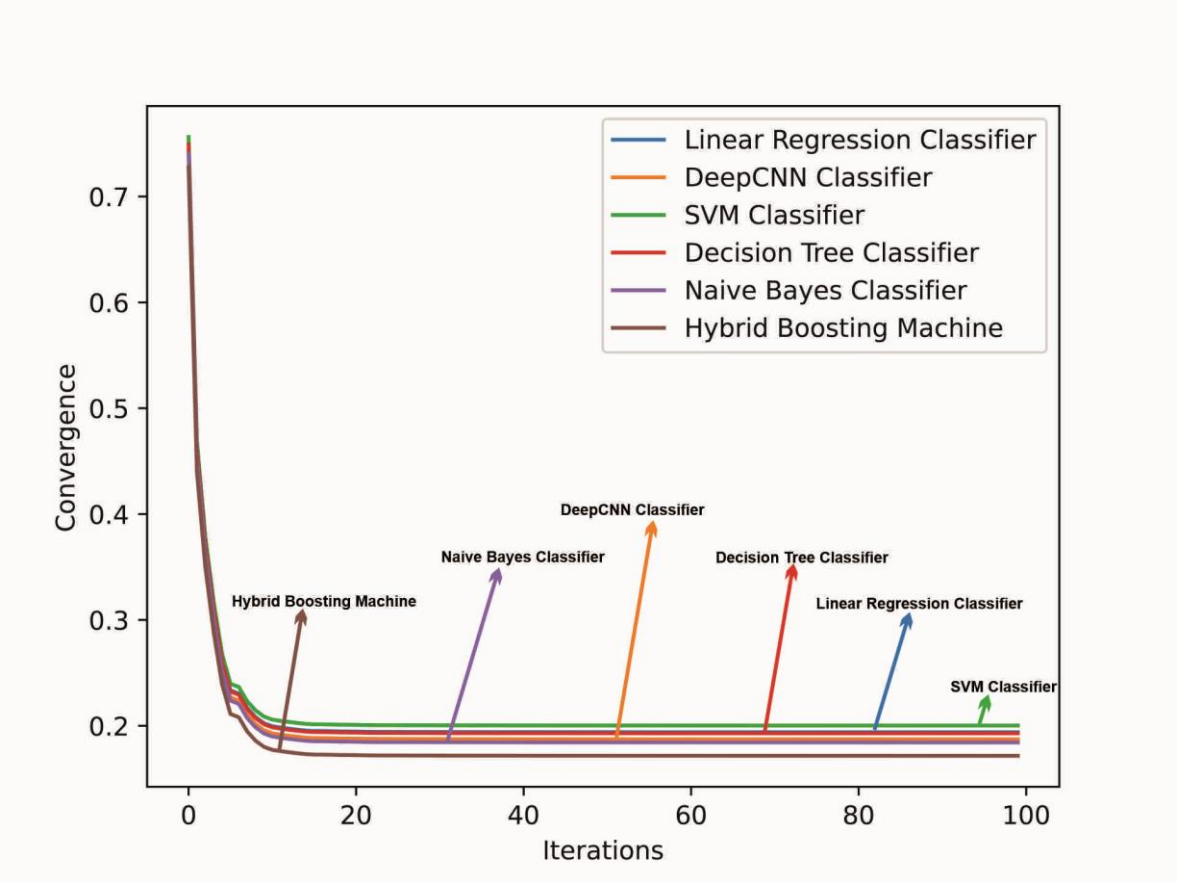

a) Convergence analysis on the DSO-1

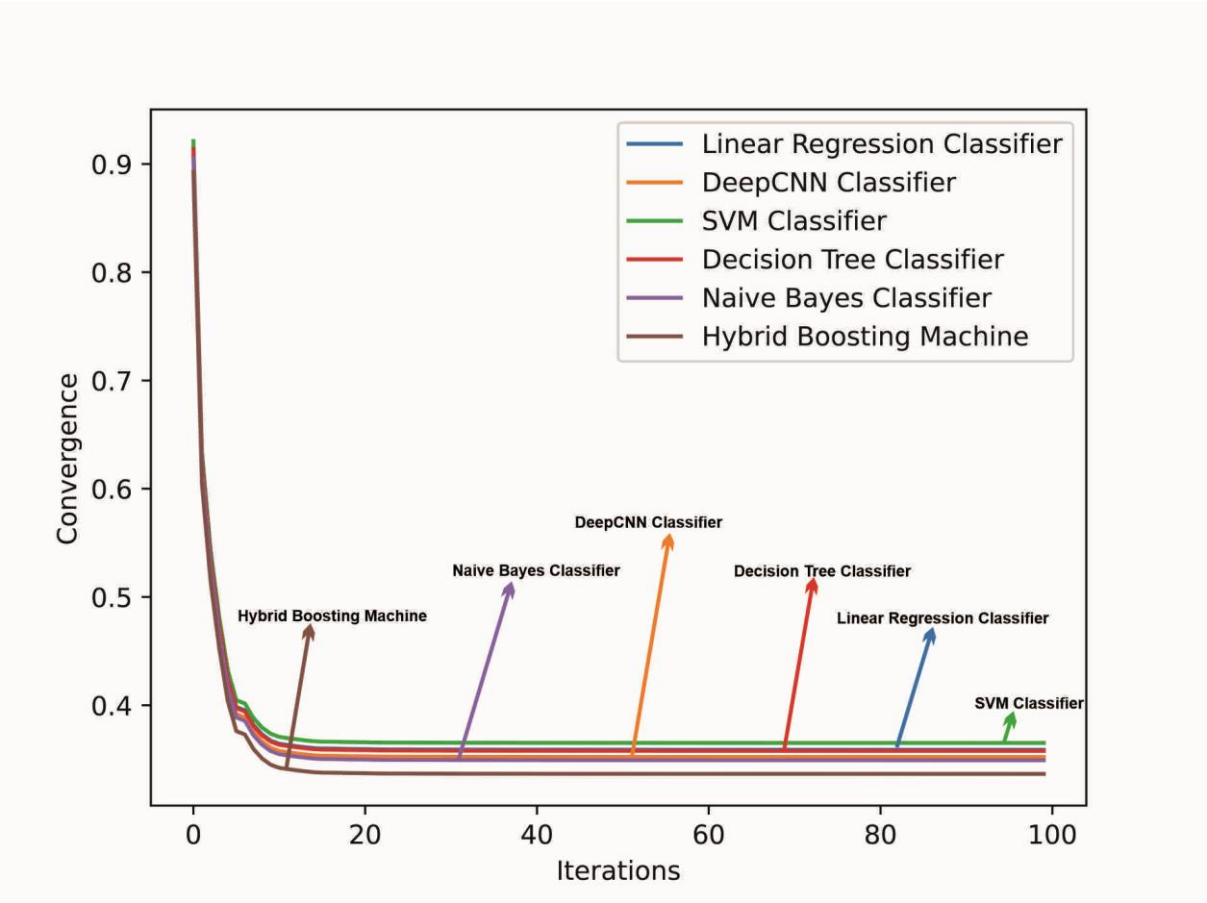

b) Convergence analysis on the DSI-1

Fig 12. Convergence Analysis of the Hybrid Boosting Machine Model

VII. Time Complexity Analysis

The time complexity analysis of the Hybrid Boosting Machine technique based on datasets DSO-1 and DSI-1 is illustrated in Fig. 11. Here, the comparison between the Hybrid Boosting Machine model and existing techniques based on computational time across various iterations is done to prove the superiority of the Hybrid Boosting

Machine model. Further, the developed technique attains a low computational time of 20.61 for DSO-1 and 20.74 for DSI-1 at iteration 100, which is faster than all other existing methods. The results emphasize the computational efficiency of the Hybrid Boosting Machine technique by showing that it consistently takes a much shorter amount of time than other existing methods. The comparison of the computational time on datasets DSO-1 and DSI-1 is depicted in Table X.

VIII. Convergence Analysis

Fig. 12 shows the analysis of convergence for the proposed Hybrid Boosting Machine approach and other traditional approaches. Here, the analysis is done by assessing the error obtained for 0 to 100 iterations. The Hybrid Boosting Machine technique achieved an error of 0.1716 for DSO-1 and 0.34 for DSI-1 at the 100th iteration, which are significantly lower than other conventional methods that achieved errors of 0.19 for LR, 0.18 for deep CNN, 0.20 for SVM, 0.19 for DT, and 0.18 for NB on DSO-1 as well as 0.36 for LR, 0.35 for deep CNN, 0.37 for SVM, 0.36 for DT, and 0.34 for NB on DSI-1. The model's efficacy and resilience in forgery detection are demonstrated by its low error rate when compared to other traditional techniques. Table XI shows the comparison of the convergence on the datasets DSO-1 and DSI-1.

IX. Conclusion

To detect image fabrications, this paper proposes a Pixel-Based Optimized Deep-CNN classification and Hybrid Boosting Machine method. Additionally, it describes a common structure for Hybrid Boosting Machine boosting a criterion method using a hybrid boosting segmentation method, similar to the standard logistic regression technique along with block-wise feature extraction, which is a process based on a block-by-block manner. The performance analysis shows that the Hybrid Boosting Machine technique achieved an accuracy of 94.74%, 95.00% sensitivity, and 95.27% specificity based on the DSO-1 as well as accuracy of 94.86%, 94.97% sensitivity, and 93.38% specificity based on DSI-1 concerning the TP. Further, the Hybrid Boosting Machine model was compared with several existing techniques, including the LR classifier, Deep-CNN classifier, SVM classifier, DT classifier, and NB classifier, and attained high accuracy, sensitivity, and specificity values of 95.14%, 95.63%, and 94.76% on the DSO-1 and 95.59%, 94.26%, and 95.59% on DSI-1 concerning the k-fold analysis. To enhance the forgery detection in the future, other hybrid DL classifiers will be used.

References

[1] Kadam, Kalyani, Swati Ahirrao, Ketan Kotecha, and Sayan Sahu, "Detection and localization of multiple images splicing using MobileNet V1," IEEE, vol. 9, pp. 162499-162519, 2021.

[2] Ding, Hongwei, Leiyang Chen, Qi Tao, Zhongwang Fu, Liang Dong, and Xiaohui Cui, "DCU-Net: a dual-channel U-shaped network for image splicing forgery detection," Neural computing and applications, vol. 35, no. 7, pp. 5015-5031, 2023.

[3] Xiao, Bin, Yang Wei, Xiuli Bi, Weisheng Li, and Jianfeng Ma, "Image splicing forgery detection combining coarse to the refined convolutional neural network and adaptive clustering," Information Sciences, vol. 511, pp. 172-191, 2020.

[4] Liu, Bo, Ranglei Wu, Xiuli Bi, Bin Xiao, Weisheng Li, Guoyin Wang, and Xinbo Gao, "D-Net: A Dual-encoder Network for Image Splicing Forgery Detection and Localization," arXiv preprint arXiv:2012.01821, 2020.

[5] Jaiprakash, Sahani Pooja, Madhavi B. Desai, Choudhary Shyam Prakash, Vipul H. Mistry, and Kishankumar Lalajibhai Radadiya, "Low dimensional DCT and DWT feature-based model for detection of image splicing and copy-move forgery," Multimedia Tools and Applications, vol. 79, pp. 29977-30005, 2020.

[6] Bi, Xiuli, Zhipeng Zhang, Yanbin Liu, Bin Xiao, and Weisheng Li, "Multi-task wavelet corrected network for image splicing forgery detection and localization," In 2021 IEEE International Conference on Multimedia and Expo (ICME), IEEE, pp. 1-6, 2021.

[7] Kumar, Avinash, Choudhary Shyam Prakash, Sushila Maheshkar, and Vikas Maheshkar, "Markov feature extraction using enhanced threshold method for image splicing forgery detection," In Smart Innovations in Communication and Computational Sciences: Proceedings of ICSICCS, Springer Vol. 2, pp. 17-27. 2019.

[8] Kaur, Navneet, Neeru Jindal, and Kulbir Singh, "A passive approach for the detection of splicing forgery in digital images," Multimedia Tools and Applications, vol. 79, pp. 32037-32063, 2020.

[9] Joseph RM, and Chithra AS, "Literature survey on image manipulation detection," International Research Journal of Engineering and Technology (IRJET), vol. 2, no. 04, pp. 2395-0056, 2015.

[10] Wu Y, Abd-Almageed W, and Natarajan P, "Deep matching and validation network: an end-to-end solution to constrained image splicing localization and detection," In Proceedings of the 25th ACM International Conference on Multimedia, pp. 1480-1502, 2017.

[11] Zhu X, Qian Y, Zhao X, Sun B, and Sun Y, "A deep learning approach to patch-based image inpainting forensics," Signal Processing Image Communication, vol. 67, pp. 90-99, 2018.

[12] Gang Cao, Yao Zhao, Rongrong Ni, and Xuelong Li, "Contrast enhancement-based forensics in digital images," IEEE Transactions on Information Forensics and Security, vol. 9, no. 3, pp. 515-525, 2014.

[13] Chenglong Chen, Jiangqun Ni, Zhaoyi Shen, and Yun Qing Shi, "Blind forensics of successive geometric transformations in digital images using the spectral method: theory and applications," IEEE Transactions on Image Processing, vol. 26, no. 6, pp. 2811-2824, 2017.

[14] DSO-1 and DSI-1 Datasets, https://recodbr.wordpress.com/code-n-data/#dso1_dsi1, Accessed on May 2023.

[15] D. Ö. Şahın, S. Akleylek and E. Kiliç, "LinRegDroid: Detection of Android Malware Using Multiple Linear Regression Models-Based Classifiers," in IEEE Access, vol. 10, pp. 14246-14259, 2022.

[16] Nath, S. and Naskar, R., "Automated image splicing detection using deep CNN-learned features and ANN-based classifier." Signal, Image and Video Processing, 15, pp.1601-1608, 2021.

[17] Ahlawat, Savita, and Amit Choudhary. "Hybrid CNN-SVM classifier for handwritten digit recognition." Procedia Computer Science 167, pp. 2554-2560, 2020.

[18] Khraisat, Ansam, Iqbal Gondal, Peter Vamplew, Joarder Kamruzzaman, and Ammar Alazab. "Hybrid intrusion detection system based on the stacking ensemble of c5 decision tree classifier and one class support vector machine." Electronics vol. 9, no. 1: 173, 2020.

[19] P. Valdiviezo-Diaz, F. Ortega, E. Cobos and R. Lara-Cabrera, "A Collaborative Filtering Approach Based on Naïve Bayes Classifier," in IEEE Access, vol. 7, pp. 108581-108592, 2019.

[20] Mniai, A., & Jebari, K., "Credit card fraud detection by improved SVDD", in Proceedings of the World Congress on Engineering, pp. 6-8, 2022.

[21] Miyajima, H., Shigei, N., Miyajima, H., & Shiratori, N. "Securely Distributed Computation with Divided Data for Particle Swarm Optimization", in Lecture Notes in Engineering and Computer Science: Proceedings of The International MultiConference of Engineers and Computer Scientists, pp. 20-22, 2021.

[22] Kang Tan, Linna Li, and Qiongdan Huang, "Image Manipulation Detection Using the Attention Mechanism and Faster R-CNN", IAENG International Journal of Computer Science, vol. 50, no. 4, pp.1261-1268, 2023.